SPANDIDOS PUBLICATIONS

ONCOLOGY LETTERS 20: 201, 2020

Morphological and functional alterations of the prostate tissue during clinical progression in hormonally-naïve, hormonally-treated and castration-resistant patients with metastatic prostate cancer

MICHAL KORČEK[1], MONIKA SEKEREŠOVÁ[2], ALEXANDER V. MAKAREVICH[3], HELENA GAVUROVÁ[2], LUCIA OLEXÍKOVÁ[3], JURAJ PIVKO[3] and LENKA BARRETO[1]

Departments of [1]Urology and [2]Pathology, Faculty Hospital Nitra, 94901 Nitra; [3]Research Institute for Animal Production Nitra, National Agricultural and Food Centre, 95141 Lužianky-near-Nitra, Slovak Republic

Received July 15, 2019; Accepted March 26, 2020

DOI: 10.3892/ol.2020.12064

Abstract. Since commony used tools in oncological practice for the diagnosis of castration-resistent prostatic acinar adenocarcinoma are based on clinical criteria, such as castrate testosterone level, continuous rise in serum prostate-specific antigen, progression of preexisting disease or appearance of new metastases, it is important to identify reliable histopathological markers for the identification of this disease. Therefore, the aim of the present study was to determine the association between results from histological analysis, ultrastructural analysis and apoptosis in the prostate of patients with metastatic acinar prostatic adenocarcinoma (mPC). Patients were treated with androgen deprivation therapy (ADT), abiraterone acetate (Abi) therapy or received no treatment. Prostate tissue samples were divided into four groups as follows: i) Group 1, tissues from patients with benign prostatic hyperplasia (adenocarcinoma negative); ii) group 2, tissues from patients with metastatic hormone naïve prostate cancer; iii) group 3, tissues from patients with mPC treated with ADT; and iv) group 4, tissues from patients with metastatic castration-resistant prostate cancer treated with ADT and Abi. Immunohistochemical, terminal deoxynucleotidyl-transferase-mediated dUTP nick end labelling (TUNEL) and ultrastructural assays using light, fluorescence and transmission electron microscopy, respectively, were used to analyze prostate tissue samples. The results demonstrated that ADT and Abi therapy caused histological and ultrastructural changes in prostate tissues. In groups 3 and 4, benign and malignant tissues were affected by the hormonal therapy. Histologically, the malignant epithelium after ADT therapy in groups 3 and 4 presented with a loss of glandular architecture, nuclear and nucleolar shrinkage, chromatin condensation and cytoplasmic clearing. At the ultrastructural level, compact hypertrophic and hyperchromatic nuclei with numerous invaginations were observed in groups 2, 3 and 4. In addition, the incidence of abnormal mitochondria in malignant cells of these groups was high. Group 4 was characterized by the presence of malignant mesenchyme-like cells in the prostatic stroma, arranged in small groups surrounded by collagen fibrils. Furthermore, the cytoplasm of these cells contained filaments. A decrease in the number of apoptotic cells using TUNEL assays in the examined samples was observed with increasing disease progression. The findings from the present study suggest that the duration of treatment with ADT and progression of the disease were associated with apoptosis dysregulation.

Correspondence to: Dr Alexander V. Makarevich, Research Institute for Animal Production Nitra, National Agricultural and Food Centre, Hlohovecka 2, 95141 Lužianky-near-Nitra, Slovak Republic
E-mail: makarevic@vuzv.sk

Key words: prostate cancer, histology, ultrastructure, apoptosis, therapy

Introduction

In 2018, prostate cancer was the second most common malignancy and the fifth leading cause of cancer-associated mortality in men worldwide (1). The incidence differs by >25-fold among regions, with the highest incidence being in Australia/New Zealand and the lowest in South-Central Asia (1).

According to the World Health Organization (WHO), acinar adenocarcinoma is an invasive carcinoma that consists of neoplastic prostatic epithelial cells with secretory differentiation arranged in a variety of histomorphological patterns, including glands, cords, single cells and sheets, and basal cells are typically absent (2). Antibodies against high molecular weight cytokeratin (HMW-CK) and p63 may identify basal cells, and α-methylacyl-CoA racemase (AMACR) is a positive marker for acinar adenocarcinoma (2-4). In high-grade acinar adenocarcinoma, it is crucial to use antibodies against cytokeratin 7 (CK7), CK20

and prostate-specific antigen (PSA) to identify whether the tumor derives from the colon, rectum, urinary bladder or a metastatic disease (5,6). Gleason grading system is used for the prognosis of prostate acinar adenocarcinoma. This standard method is used worldwide to grade prostate cancer, and is based on the degree of architectural differentiation (4,7,8). For therapeutic purposes, a new prognostic grading group has been developed and is applied in conjunction with the 2014 WHO/International Society of Urologic Pathologists (9-11). The Gleason grading system should not be applied in case of the therapy effect (2).

Androgen deprivation therapy (ADT) is a treatment that alters the benign and cancerous prostatic epithelium by inducing apoptosis, which is characterized by the fragmentation of tumor DNA (12). The histological features of the epithelium from the glandular component of prostatic carcinoma following ADT include the loss of glandular architecture, nuclear and nucleolar shrinkage, nuclear hyperchromasia and pyknosis and mucinous degeneration (13). In addition, acinar atrophy, reduced ratio of acini to stroma, enlargement and clearing of cytoplasm, prominent clear cell change, basal cell hyperplasia and increase in squamous metaplasia are also observed, following ADT. The histological changes in the prostatic stroma following ADT include an edema at early stages, fibrosis at late stages and patchy condensation of the stroma resulting in focal hypercellularity and focal chronic lympho-histiocytic inflammation (13,14).

Ultrastructural changes of prostate cancer cells compared with normal or hypertrophic prostate cells are well known and have been reported by numerous researchers (15-18). It has been demonstrated that cancer prostate secretory cells present with hyperchromatosis of the nucleus, hypertrophy of the nucleus and nucleolus, an increased number of pleiomorphic mitochondria, various configurations and positions of Golgi complexes and increased amount of lipid droplets of different morphology (15). In prostate cancer cells, an increase in the number of mitochondria of different morphology has been reported in patients with a high degree of prostate malignancy according to the Gleason score (18).

Apoptosis, or programmed *in situ* cell death, is a physiological homeostatic mechanism involving cell death that naturally occurs during normal tissue turnover (19,20). Apoptosis dysregulation serves a crucial role in numerous pathological processes, including inflammation, hyperplasia, cancer and responses to therapy (21). Molecular imaging of apoptotic cells could therefore be useful for early detection of anticancer therapy effects (22-24). Apoptosis in acinar adenocarcinoma was described in small foci of prostate cancer cells (2,3). Previous studies on apoptosis in prostatic carcinoma reported a positive association between the amount of apoptotic bodies and Gleason grade (25-29).

The present study aimed to characterize the complex structural processes that occur in the malignant prostate through histological, immunohistochemical (IHC) and ultrastructural analyses using light, fluorescence and transmission electron microscopy, in order to determine the importance of assessing individual histological structures of the prostate in the clinical course of the disease. To do so, prostate acinar adenocarcinoma tissues from newly-diagnosed naïve patients with metastatic disease, patients treated with ADT alone, or with ADT and abiraterone acetate (Abi) were collected.

Materials and methods

Ethical approval. The Ethics Commission of the Faculty Hospital Nitra (Nitra, Slovak Republic) approved the present study. All patients provided written informed consent.

Patients and samples. Prostate tissue samples were collected between November 2016 and June 2017 during transurethral resection from 22 patients with bladder outlet obstruction and histologically confirmed benign prostatic hyperplasia (BPH) and acinar adenocarcinoma prostate cancer at the Faculty Hospital Nitra (Nitra, Slovak Republic). At the time of surgery, the mean age of the patients was 70.7 years (age range, 58-85 years). Based on the Tumor-Node-Metastasis (7th edition) clinical stage (30) and the type of treatment, samples were divided into four groups as follows: i) Group 1, samples from patients with BPH (adenocarcinoma-negative); ii) group 2, samples from patients with metastatic hormone naïve acinar prostatic adenocarcinoma (mHNPC); iii) group 3, samples from patients with metastatic acinar prostatic adenocarcinoma (mPC) and receiving ADT; and iv) group 4, samples from patients with metastatic castration-resistant acinar prostatic adenocarcinoma (mCRPC) and receiving ADT and Abi therapy (Table I). The patient clinicopathological characteristics and the number of patients in each group are presented in Table I. Patients in group 3 were treated with leuprorelin acetate (5 mg subcutaneously every 3 months) ADT drug for an average duration of 36 months (duration range, 6-80 months). Patients in group 4 were treated with leuprorelin acetate (5 mg subcutaneously every 3 months) ADT drug for an average duration of 50 months (duration range, 47-60 months). In groups 3 and 4 there was no statistically significant differences in the length of ADT treatment (P=0.40). Patients from group 4 also received abiraterone acetate, a standard treatment for mCRPC, orally at a dose of 1,000 mg/day fasting for an average treatment duration of 15 months (duration range, 3-27 months). At the time of tissue collection, patients in groups 3 and 4 had castrated testosterone levels (<50 ng/dl) (31) due to being treated with ADT. Additionally, patients in group 3 did not have clinical or biochemical signs of cancer progression, and patients in group 4 with CRPC continuing with ADT and Abi therapy, as is standard treatment (31), did not have signs of clinical progression.

Histological and IHC analyses. The histological diagnosis was determined following conventional biopsy. Fresh tissue samples following collection were fixed in 10% neutrally-buffered formaldehyde solution for 24 h at room temperature, dehydrated in an ascending ethanol series (80, 90 and 100%) at room temperature, and embedded in paraffin. Paraffin sections of 5-μm thickness were prepared using a microtome. Sections for histological analysis were stained with Mayer's hematoxylin and eosin in Dako CoverStainer (Dako; Agilent Technologies, Inc.) at room temperature for 20 min. Sections for IHC analysis were deparaffinized and rehydrated in the automatic pre-treatment module PT Link (Dako; Agilent Technologies, Inc.) at 97˚C for 40 min. Sections were inserted into DakoAutostainer 48 Link, and the required protocols were selected according to the manufacturer's instructions. Sections were incubated with primary atibodies against HMW-CK (cat. no. IR051), AMACR (cat. no. IR060), PSA

Table I. Clinicopathological characteristics of patients according to TNM classification.

Groups	T3-4, n	N+, n	M+, n	PSA level, ng/ml (range)
BPH (n=5)	N/A	N/A	N/A	9.30 (0.66-17.65)
mHNPC (n=6)	6	2	6	88.00 (45.00-154.00)
mPC + ADT (n=6)	6	2	6	8.55 (1.19-22.40)
mCRPC + ADT + Abi (n=5)	5	3	5	91.98 (45.90-131.00)

Abi, abiraterone acetate; ADT, androgen-deprivation therapy; BPH, benign prostatic hyperplasia; mCRPC, metastatic castration-resistant prostate cancer; mHNPC, metastatic hormone naïve prostate cancer; mPC, metastatic acinar prostatic adenocarcinoma; n, number of patients. PSA, prostate specific antigen; T3-4, locally extended disease; TN, total number of patients; N+, spread of cancer to lymph nodes; M+, presentation of distal metastasis; TNM, Tumor-Node-Metastasis; N/A, not applicable.

(cat. no. IR514), CK7 (cat. no. IR619) and CK20 (cat. no. IR777) at room temperature for 20 min, and subsequently with EnVision™ Flex/HRP secondary antibody (cat. no. K8000) at room temperature for 20 min (all Dako; Agilent Technologies, Inc.). All primary and secondary antibodies were ready to use (undiluted). The visualization step was performed with EnVision™ Flex/DAB and Chromogen (cat. no. K8000) for 10 min, subsequently washed with water for 5 min. Sections were stained with Mayer's hematoxylin for 5 min at room temperature. Finally, sections were rehydrated in a descending ethanol series (100, 90 and 80%), cleared with 99% xylene and mounted with DAKO Toluene-free mounting medium (Dako; Agilent Technologies, Inc.). Sections were observed using a Nikon Eclipse Ci-L light microscope (magnification, x200; Nikon Corporation), and images were digitally recorded using an Imaging Source camera (The Imaging Source Europe GmbH). Samples from group 2 (patients with mHNPC) were evaluated using the Gleason grading of prostatic carcinoma (9).

Electron microscopic analysis. Fresh prostatic tissue samples immediately after collection were fixed in an aldehyde mixture containing 2.5% glutaraldehyde and 2% paraformaldehyde in 0.1 M sodium cacodylate buffer at pH 7.2-7.4 at 4˚C for 1 h and subsequently post-fixed in 1% osmium tetroxide dissolved in 0.1 M sodium cacodylate for 1 h at room temperature. Following dehydration in an ascending acetone series (30, 50, 70, 80, 90, 95 and 100%), samples were embedded into Poly/Bed Embedding Media (Polysciences, Inc.). Ultrathin sections of 70-nm thickness were cut using a Leica EM UC6 ultra microtome (Leica Microsystems GmbH) and contrasted with 10% uranyl acetate solution dissolved in absolute methanol and lead citrate according to methods by Reynolds (32), in order to visualize cellular organelles. The contrasted sections were imaged using a JEM100 CXII transmission electron microscope (JEOL, Ltd.) at an accelerating voltage of 80 kV and a magnification range between x1,900 and x7,200.

Fluorescent determination of apoptosis using terminal deoxynucleotidyl-transferase-mediated dUTP nick end labelling (TUNEL) assay. Paraffin-embedded prostatic tissue sections (5 μm) previously fixed in 10% neutrally-buffered formalin were analyzed using TUNEL assay, using *In Situ* Cell Death Detection kit, Fluorescein (Roche Diagnostics GmbH) according to the manufacturer's instructions. The samples were deparaffinized using pure xylene (≥99%), rehydrated in a descending ethanol series (100, 90 and 80%) and permeabilized using proteinase K (Roche Diagnostics GmbH). Sections were labelled with TdT-reagent for 60 min in a wet chamber at 37˚C in a thermostat. Sections were covered with a Vectashield anti-fade medium (Vector Laboratories, Inc.) and mounted into a sandwich between a microslide and a coverslip. Presence of apoptotic cells was analyzed under a Leica fluorescence microscope (Leica Microsystems GmbH) equipped with a digital camera DFC-480 with a total magnification of x220. For the positive control, sections were treated with 1,500 U/ml recombinant DNase I (Roche Diagnostics GmbH) prior to TdT labelling and incubated in a humidified atmosphere for 60 min at 37˚C in the dark. For the negative control, sections were incubated only with a fluorescein isothiocyanate-labelling solution, according to the manufacturer's protocol (*In Situ* Cell Death Detection kit; Roche Diagnostics GmbH), in the absence of TdT-reagent for 60 min at 37˚C in the dark (data not shown).

Following TUNEL assay, apoptotic cells and fragments exhibited green fluorescence on a dark background. The distribution of apoptosis in the examined samples was different in all 4 groups. In each sample, in areas where apoptosis occurred, images were taken from 10 fields of view at x200 magnification (ocular, x10; objective, x20) under a fluorescence microscope. The number of apoptotic cells was manually counted and statistically analyzed.

Statistical analysis. ANOVA followed by least significant difference post hoc test was used to analyze the difference in the number of apoptotic cells between the 4 groups. Data were analyzed using SPSS Statistics software (version 20; IBM Corp.). The level of α significance was determined at 0.05, and $P<0.05$ was considered to indicate a statistically significant difference. One-way ANOVA followed by Tukey's post hoc test was used for comparisons among multiple groups. The differences in the number of apoptotic cells between all groups were evaluated. The calculated values were plotted in a dot graph.

Results

Histology and ultrastructure of BPH samples. Histologically, BPH tissue from group 1 was formed by dilated hyperplastic

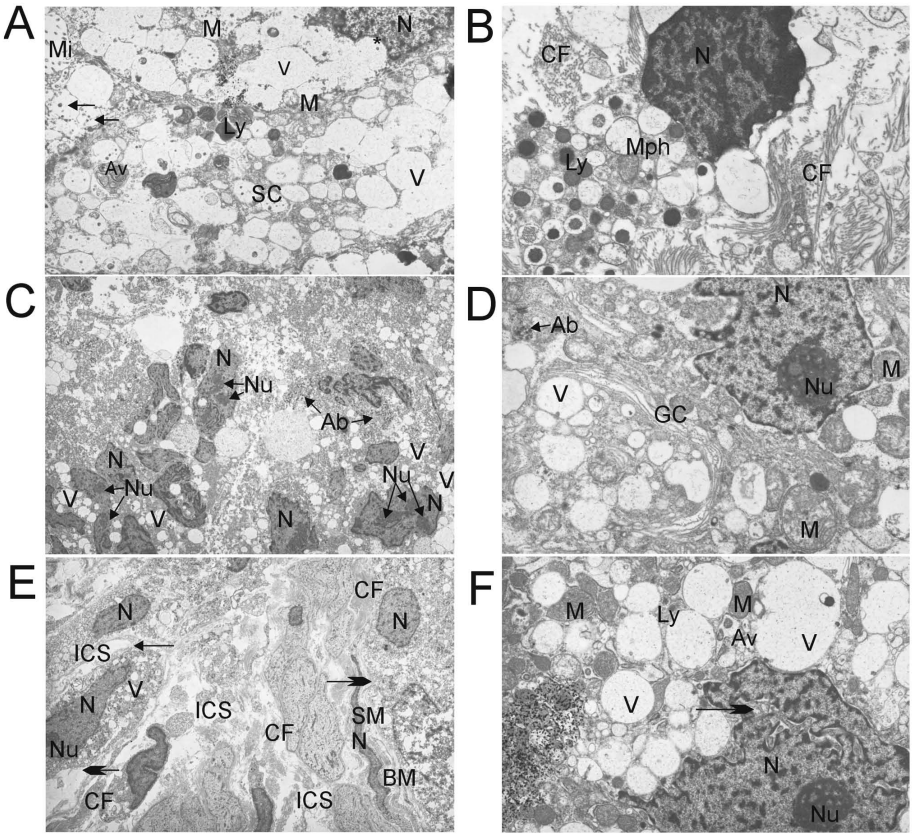

Figure 1. Ultrastructural analysis of prostate tumor tissue by EM. (A) EM analysis of benign prostatic hyperplasia tissue (group 1) showing the supranuclear region of SC with Mi oriented into the lumen of acinus, M, large V of the endoplasmic reticulum, Ly, N with invagination (asterisk) and secretory granules (arrows). Primary magnification, x4,800. (B) EM analysis of benign prostatic hyperplasia tissue (group 1) showing Mph in the stroma of the prostate tissue with dense N, numerous Ly and CF around. Primary magnification, x7,200. (C) EM analysis of metastatic hormone naïve prostate cancer tissue (group 2) showing disintegrated acini with hyperchromatic N and prominent Nu, assumed Ab near the N, and V of endoplasmic reticulum. Primary magnification, x1,900. (D) EM analysis of metastatic acinar adenocarcinoma tissue following ADT (group 3) showing hyperchromatic N, Nu, abnormal and swollen M with disrupted cristae, cisternae of GC, V of the endoplasmic reticulum and probably Ab. Primary magnification, x7,200. (E) EM analysis of metastatic castration-resistant prostate cancer tissue following ADT and Abi treatment (group 4) showing solitary malignant cells with small N and hypertrophic Nu. V of the endoplasmic reticulum are less present compared with group 1 (Fig. 1A), and secretory granules are not visible. Apical-basal cell polarity was lost, intercellular joints were disrupted (small arrow), ICSs were dilated and the BM was degraded (big arrows). These secretory cells appeared as mesenchymal-like cells. There are also abundant CF and SM cells with N. Primary magnification, x1,900. (F) EM analysis of metastatic castration-resistant prostate cancer tissue following ADT and Abi treatment (group 4) showing N with deep invagination (arrow), compact Nu, electron-dense M, large V of the endoplasmic reticulum, Ly and Av. Primary magnification, x7,200. Abi, abiraterone acetate; ADT, androgen-deprivation therapy; EM, electron microscopy; M, mitochondria; N, nucleus/nuclei; Nu, nucleoli; Mi, microvilli; V, vesicles; Ly, lysosomes; Mph, macrophages; CF, collagen fibrils; Ab, apoptotic body; GC, Golgi complex; ICS, intercellular space; BM, basal membrane; SM, smooth muscle; AV, autophagic vacuoles; SC, secretory cell.

glands with two layers, epithelial and myoepithelial. This was verified in one case (sample 5) following IHC examination with HMW-CK and AMACR. The basal cell layer was positive for the HMW-CK antibody, whereas the epithelial layer was negative for the AMACR antibody. In two samples (no. 13 and 14), in addition to gland hyperplasia, chronic active prostatitis with periglandular chronic inflammatory infiltrate and presence of neutrophil leukocytes in the lumen of the glands was detected (data not shown).

Ultrastructurally, in the case of BPH (group 1), well-developed microvilli were visible on the luminal surface of the cells. The epithelial secretory cells were cylindrical in shape and were attached to the basal membrane along with the small basal cells (data not shown). The cytoplasm of the secretory cells contained supranuclearly positioned secretion granules, oval mitochondria, prominent and numerous vesicles of granular endoplasmic reticulum, which were often expanded in the supranuclear area and surface parts. Heterochromatic nuclei had an oval shape and the nucleoli were of a reticular form. Some nuclei were hyperchromatic and had numerous invaginations and signs of degeneration. The incidence of compact nucleoli, swollen mitochondria and lysosomes was low (Fig. 1A). The stroma was sporadically occupied with macrophages (Fig. 1B).

Histology and ultrastructure of samples from patients with metastatic acinar adenocarcinoma following ADT or not. Samples from patients with acinar adenocarcinoma and who did not receive treatment (group 2) presented with small glands in a random arrangement, hyperchromatic nuclei and prominent nucleoli, amphophilic cytoplasm without basal cell layer, according to IHC staining for AMACR-positivity and HMW-CK negativity (data not shown). The Gleason score was determined according to this architectural pattern (3+3, 3+4, 5+5). In the samples from group 3 (patients who received ADT), groups of individually arranged cells with round-shaped nuclei and light cytoplasm were observed as a treatment effect (data not shown). Since the Gleason score is not recommended to be applied in patients subjected to ADT (2,33), the Gleason score was not used as a criteria in the present study.

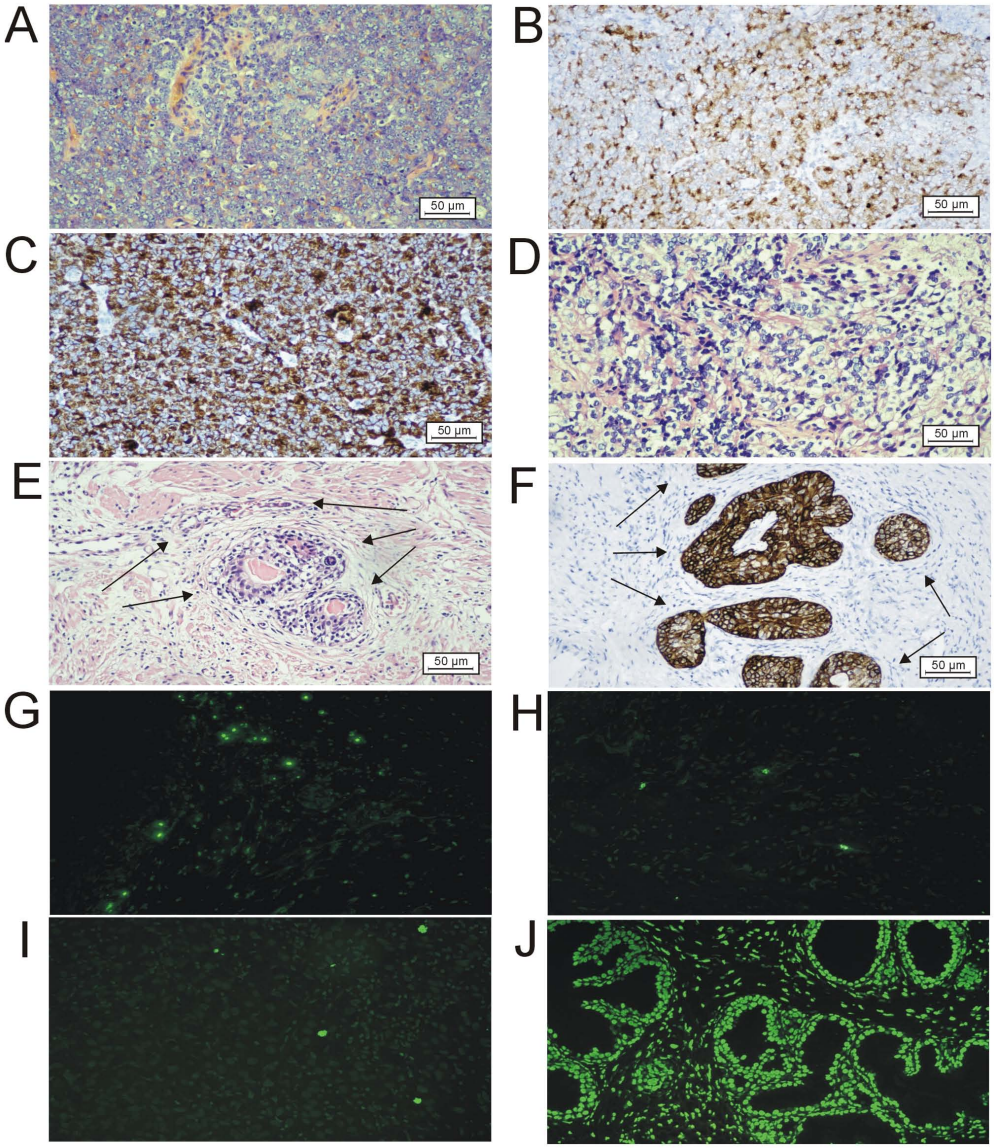

Figure 2. Histological, immunohistochemical and apoptotic images of prostatic tumor tissues. (A) Solid vital tumor following ADT in group 4 (HE staining). Scale bar, 50 μm. (B) Prostate-specific antigen-positive staining using IHC in group 4. Scale bar, 50 μm. (C) α-Methylacyl-CoA racemase-positive staining using IHC in group 4. Scale bar, 50 μm. (D) Histological image of HE staining of the ADT therapeutic effect in group 4, showing nuclear hyperchromasia and pyknosis, nuclear shrinkage and clear cytoplasm. Scale bar, 50 μm. (E) Histological image of HE staining of benign glands with basal cell hyperplasia (arrows) and enlargement and clearing of the cytoplasm (group 4). Scale bar, 50 μm. (F) High molecular weight cytokeratin positive staining using IHC demonstrating basal cell hyperplasia (arrows) in benign glands (group 4). Scale bar, 50 μm. (G) TUNEL assay on sample no. 19 (group 2) of metastatic hormone naïve prostate cancer showing 10 apoptotic cells in one field of view in the malignant glandular epithelium. Magnification, x200. (H) TUNEL assay on sample no. 25 (group 3) of metastatic acinar adenocarcinoma with androgen deprivation therapy, showing 4 apoptotic cells in one field of view in a solidly arranged glandular epithelium. Magnification, x200. (I) TUNEL assay on sample no. 27 (group 4) of metastatis castration-resistant prostate cancer following ADT and abiraterone acetate treatment showing 3 apoptotic cells in one field of view in malignant glandular epithelium. Magnification, x200. (J) Positive control for TUNEL assay (treated with recombinant DNase I). Magnification, x200. HE, hematoxylin-eosin; IHC, immunohistochemistry; ADT, androgen-deprivation therapy; TUNEL, terminal deoxynucleotidyl-transferase-mediated dUTP nick end labelling.

The ultrastructural images of samples from the groups 2 and 3 were similar and were characterized by the presence of secretory cells without basal cells. In both groups, disintegrated acinus and hyperchromatic nuclei were identified; the nuclei presented with an oval shape with numerous invaginations and signs of degeneration. In addition, the hypertrophic nuclei were of compact form and high in number. The granular endoplasmic reticulum and Golgi complex presented with similar structures in the two groups. In group 2, some apoptotic bodies were identified (Fig. 1C). Furthermore, the number of swollen mitochondria with altered cristae morphology in secretory cells of samples from the group 3 was high (Fig. 1D). Impaired integrity of the basal membrane was observed in samples from the 4 groups.

Histology and ultrastructure of samples from patients with mCRPC who received ADT and Abi treatment. Histologically mCRPC (group 4) was characterized by solid and solid-alveolar arranged foci (33) of malignant cells with hyperchromatic nuclei and prominent nucleoli, small to moderate amount of amphophilic cytoplasm, a shift of the nucleus/cytoplasm ratio and numerous mitoses, including atypical mitoses (Fig. 2A). Locally, foci of glandular formation were noted. IHC staining

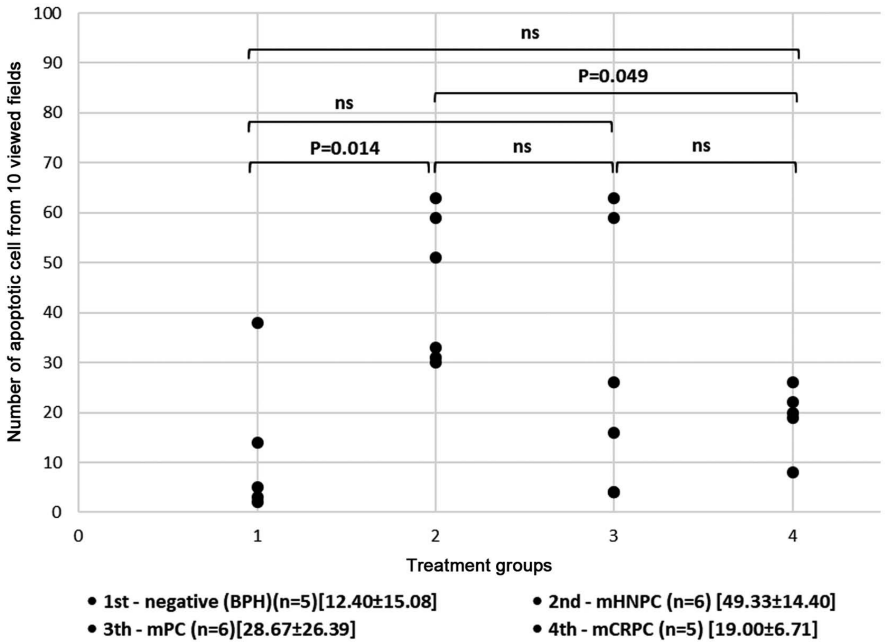

Figure 3. Number of apoptotic cells in the 4 groups of samples. Mean ± SD values are shown in square brackets. Abi, abiraterone acetate; ADT, androgen-deprivation therapy; BPH, benign prostatic hyperplasia; mCRPC, metastatic castration-resistant prostate cancer; mHNPC, metastatic hormone naïve prostate cancer; mPC, metastatic acinar prostatic adenocarcinoma; ns, not significant.

of malignant cells revealed positivity for PSA and AMACR (Fig. 2B and C, respectively). IHC staining of the myoepithelial layer with HMW-CK and staining for CK7 and CK20 was negative (data not shown). A portion of the malignant cells were arranged in clusters, rows, or as single cells (34), and presented with a lightly stained eosinophilic cytoplasm and small hyperchromatic nuclei as a sign of the therapeutic effect (Fig. 2D). As aforementioned, the Gleason score was not determined.

Benign glands with basal cell hyperplasia were also identified in group 4, as confirmed by the IHC positivity for HMW-CK (Fig. 2E). Basal cells in the benign glands manifested enlargement and clearing of the cytoplasm following treatment compared with the untreated BPH (Fig. 2E and F).

Ultrastructurally, mCRPC, in comparison with naïve prostate cancer (group 2), was characterized by the presence of a large amount of connective tissue, smooth muscle bundles and solitary, malignant cells arranged into small groups located in the prostate stroma with prominent fibrils of collagen (Fig. 1E). The nuclei of these malignant cells were small, oval in shape and their membrane formed numerous invaginations on the inside. Chromatin in the nucleus was evenly distributed and formed hyperchromatic clusters. The nuclei contained numerous, large, predominantly compact nucleoli. The cytoplasm contained a great number of electron-dense mitochondria with altered cristae, lysosomes and autophagic vacuoles (Fig. 1F).

Determination of cell apoptosis. Apoptosis is the most common form of death in eukaryotic cells. In each group, apoptosis was observed in the glands but rarely in the stroma (Fig. 2G-I; data not shown for group 1). Apoptotic fragments also occurred in the lumen of the gland.

The results from the statistical analysis revealed that the number of apoptotic cells in the assessed fields of view was significantly increased in hormonally naïve, high-risk prostate cancer tissues compared with benign tissue samples. The one-way ANOVA test revealed significant differences among the groups (P=0.014); the post-hoc Tukey's test confirmed the significant difference in the apoptosis frequency was between group 1 (12.40±15.08) and group 2 (49.33±14.40) (P=0.014). Furthermore, the number of apoptotic cells in samples from patients who received ADT treatment (groups 3 and 4) was mainly decreased compared with patients who did not receive any treatment (group 2). Although there was no significant difference in the number of apoptotic cells between groups 2 and 3 (P=0.215; group 3 mean ± SD, 28.67±26.39), the number of apoptotic cells in group 4 was significantly decreased compared with that in group 2 (P=0.049; group 4 mean ± SD, 19.00±6.71) (Fig. 3).

Discussion

The present study demonstrated that ADT and Abi therapy (groups 3 and 4) had a therapeutic effect on the histological structure of prostate cancer cells compared with group 2 (no treatment), which was consistent with other reports (13,14). This effect was characterized by the loss of glandular architecture, nuclear hyperchromasia and pyknosis, nuclear shrinkage and a clear cytoplasm. In addition, malignant cells were arranged in clusters, rows or remained individual. Furthermore, benign prostate glands presented with basal cell hyperplasia, enlargement and clearing of the cytoplasm following ADT in both groups 3 and 4.

The changes in the ultrastructure of prostate cancer secretory cells reported in the present study were consistent with previous findings (15-18). The current study demonstrated the high incidence of hyperchromatic nuclei and compact nucleoli in prostate cancer secretory cells. Furthermore, pleiomorphic changes in the mitochondria were observed in prostate cancer secretory cells, including mitochondrial swelling and altered cristae morphology, which were associated with clinical

progression (groups 2-4). Similar to Kaighn *et al* (16), the present study reported a disruption in the integrity of the desmosomes in the prostate secretory cells from groups 3 and 4, and the presence of solitary cells in the stroma. Occurrence of hyperchromatic nuclei and compact nucleoli was high in cells from group 4 (mCRPC). In this group, an increased incidence of electron-dense, dark mitochondria with impaired cristae morphology were also identified. These morphological changes were associated with clinical progression of the disease.

Apoptosis involves numerous changes in cells, leading to the death of functionally impaired cells (19,35). In oncology, apoptosis is triggered by a variety of antitumor drugs, radiation and hyperthermia, and the intrinsic propensity of tumor cells to respond by apoptosis is modulated by expression of several oncogenes (36). Apoptosis may therefore be considered as a prognostic marker for cancer treatment (37). Numerous markers are used for the detection of apoptosis in tumor cells, including caspase-3, Annexin V, poly ADP ribose polymerase, apoptotic peptidase activating factor 1, Bax, Bid, Bcl-2, p53 tumor suppressor gene or Fas receptor (21,38). The analysis of apoptotic markers was not performed in the present study due to the small number of tissue samples from patients. Subsequently, TUNEL assay, which is based on DNA fragmentation, was used to assess apoptosis. In the present study, the functional process of apoptosis was only assessed as a final stage of cell death, which was a limitation. However, apoptosis can also be identified morphologically. Further investigation focusing on the functional and morphological determination of apoptosis may therefore be beneficial.

The present study demonstrated that the numbers of apoptotic cells between patients with BPH (group 1) and patients with mHNPC (group 2) and mCRPC (group 4) were statistically different. The association between apoptosis, mHNPC and mCRPC, despite the small sample size, has a certain scientific significance. The decrease in apoptosis incidence in tissues from patients following ADT (group 2 vs. groups 3 and 4) was consistent with a previous study (39). The differences observed between the groups were due to the third group, which was non-homogenous (treatment duration of each patient was different). Dysregulation of the apoptotic signaling pathway is associated with the progression of androgen deprivation in CRPC, which reflects the blockade of apoptosis following ADT (40). In the present study, patients treated with ADT and presenting with clinical remission (group 3) showed a high amount of variability in the incidence of apoptosis. Development of CRPC is individual and depends on the patient. The expression of numerous protein members of the Bcl-2 family, including Bcl-2, Bcl-XL and Mci-1, is highlighted during progression into a castration-resistant metastatic phenotype by losing the ability for extracellular matrix proteins to bind to the cell surface (40).

A previous study (41) reported the pathological role of the *Myb* gene, which is a transcription factor that is overexpressed in mCRPC (41). Myb promotes cell cycle progression and stimulates cell survival in androgen-supplemented and deprived conditions, respectively, through induction of Bcl-xL and Bcl2 proteins and downregulation of p27 and the pro-apoptotic protein Bax. Furthermore, Srivastava *et al* (41) reported the positive role of Myb in the enhanced motility and invasive capacity and decreased homotypic interactions of prostate cancer cells. *Myb* overexpression is also associated with actin reorganization, which leads to the formation of filopodia-like cellular protrusions that promote cell migration; furthermore, *Myb* enhances the proliferation and androgen deprivation-resistance of prostate cancer cells and confers to these cells an aggressive phenotype by facilitating the epithelial-to-mesenchymal transition (EMT) (42). Several studies have indicated a direct link between EMT and the generation and development of a tumor (43,44). Mesenchymal cells are relatively more motile and exhibit less cell-to-cell communication compared with cancer cells. Cancer cells gain mesenchymal features during their progression through EMT (42-44). At the ultrastructural level, the present study demonstrated that in cells from group 4, the apical-basal cell polarity was lost, intercellular joints were disrupted, the basal membrane was degraded and cells seemed to acquire a mesenchymal-like phenotype (42).

In conclusion, the aim of the present study was to describe the biological changes that appear during the clinical progression of metastatic prostate cancer. A combined approach including apoptosis assay, IHC, fluorescent and transmission electron microscopy was used. The results indicated that samples from patients with mPC consisted of randomly arranged glands with hyperchromatic nuclei and prominent nucleoli without basal cell layer, which was also confirmed using IHC examination of AMACR-positivity and HMW-CK-negativity and ultrastructural analysis. Furthermore, a decrease in the number of apoptotic cells was identified in end-stage prostate cancer (group 4). In addition, ADT therapy caused changes in histological structure and ultrastructure of prostate tissues. The results from the TUNEL assay following treatment suggested that the progression of the disease may be associated with apoptosis dysregulation.

Acknowledgements

The authors would like to thank Mrs. Daniela Rusevova (Department of Pathology, Faculty Hospital Nitra, Nitra, Slovak Republic) for the preparation of histological samples.

Funding

No funding was received.

Availability of data and materials

All data generated or analyzed during this study are included in this published article.

Authors' contributions

MK collected, analyzed and interpreted the patient data, and performed statistical evaluation. MS, HG, AVM, LO and JP performed the experiments. LB contributed to the analysis and the interpretation of the data, and reviewed the clinical data. All authors contributed in writing the manuscript. All authors read and approved the final manuscript.

Ethics approval and consent to participate

The present study was conducted according to the Declaration of Helsinki and approved by the Ethics Commission of the

Faculty Hospital Nitra (approval no. 11.10.2018). All patients provided written informed consent for the use of their tissue and clinical data.

Patient consent for publication

Not applicable.

Competing interests

The authors declare that they have no competing interests.

References

1. Bray F, Ferlay J, Soerjomataram I, Siegel RL, Torre LA and Jemal A: Global cancer statistics 2018: GLOBOCAN estimates of incidence and mortality worldwide for 36 cancers in 185 countries. CA Cancer J Clin 68: 394-424, 2018.
2. Moch H, Humphrey PA, Ulbright TM and Reuter VI: Tumours of the prostate. In: WHO Classification of Tumours of the Urinary System and Male Genital Organs. 4th edition. Humphrey P (ed). IARC, Lyon, pp138-162, 2016.
3. Cheng L and Bostwick DG: Urologic surgical pathology. In: E-book. Expert consult title: Online and print. 2nd edition. Elsevier Health Sciences, pp468-513, 2008.
4. Epstein JI and Netto GJ: Grading of Prostatic adenocarcinoma. In: Biopsy interpretation of the prostate. 4th edition. Pine J and McGough J (eds.) Wolters Kluwer and Lippincott Wiliams & Wilkins, pp175-198, 2008.
5. Bahrami A, Truong LD and Ro JY: Undifferentiated tumor. Arch Pathol Lab Med 132: 326-348, 2008.
6. Lin F and Liu H: Immunohistochemistry in undifferentiated neoplasm/tumor of uncertain origin. Arch Pathol Lab Med 138: 1583-1610, 2014.
7. Gleason DF: Histologic grading of prostate cancer: A perspective. Hum Pathol 23: 273-279, 1992.
8. Kryvenko ON and Epstein JI: Prostate cancer grading. Arch Pathol Lab Med 140: 1140-1152, 2016.
9. Epstein JI, Egewad L, Amin MB, Delahunt B, Srigley JR and Humphrey PA; Grading Committee: The 2014 International Society of Urological Pathology (ISUP) Consensus conference on Gleason grading of prostatic carcinoma: Definition of grading patterns and proposal for a new grading system. Am J Surg Pathol 40: 244-252, 2016.
10. Khochikar M: Newly proposed prognostic grade group system for prostate cancer: Genesis, utility and its implications in clinical practice. Curr Urol Rep 17: 80, 2016.
11. Offermann A, Hohensteiner S, Kuempers C, Ribbat-Idel J, Schneider F, Becker F, Hupe MC, Duensing S, Merseburge AS, Kirfel J, *et al*: Prognostic value of the new prostate cancer international society of urological pathology grade groups. Front Med (Lausanne) 4: 157, 2017.
12. Reuter VE: Pathological changes in benign and malignant prostatic tissue following androgen deprivation therapy. Urology 49 (Suppl 3A): S16-S22, 1997.
13. Montironi R and Schulman CC: Pathological changes in prostate lesions after androgen manipulation. J Clin Pathol 51: 5-12, 1998.
14. Bostwick DG and Meiers I: Diagnosis of prostatic carcinoma after therapy. Arch Pathol Lab Med 131: 360-371, 2007.
15. Mao P, Nakao K and Angrist A: Human prostatic carcinoma: An electron microscope study. Cancer Res 26: 955-973, 1966.
16. Kaighn ME, Narayan KS, Ohnuki Y, Lechner JF and Jones LW: Establishment and characterization of a human prostatic carcinoma cell line (PC-3). Invest Urol 17: 16-23, 1979.
17. Hernandez-Verdun D: The nucleolus: A model for the organisation of nuclear functions. Histochem. Cell Biol 126: 135-148, 2006.
18. Sun X, Liao NK and Yu JJ: Prognostic value of a mitochondrial functional score in prostate cancer. J Int Med Res 40: 371-376, 2012.
19. Kerr JFR, Wyllie AH and Currie AR: Apoptosis: A basic biological phenomenon with wide-ranging implications in tissue kinetics. Br J Cancer 26: 239-257, 1972.
20. Schmied M, Breitschopf H, Gold R, Zichler R, Rothe G, Wekerle H and Lassmannet A: Apoptosis of T lymphocytes in experimental autoimmune encephalomyelitis: Evidence for programmed cell death as a mechanism to control inflammation in the brain. Am J Pathol 143: 446-452, 1993.
21. Elmore S: Apoptosis: A review of programmed cell death. Toxicol Pathol 35: 495-516, 2007.
22. Carson DA and Ribeiro JM: Apoptosis and disease. Lancet 341: 1251-1254, 1993.
23. Gougeon ML and Montagnier L: Apoptosis in AIDS. Science 260: 1269-1270, 1993.
24. Rył A, Rotter I, Kram A, Teresiński L, Słojewski M, Dołęgowska B, Lubkowska A, Piasecka M and Laszczyńska M: Apoptosis and proliferation of the prostate cells in men with benign prostatic hyperplasia and concomitant metabolic disorders. Histol Histopathol 33: 389-397, 2017.
25. Gaffney EF: The extent of apoptosis in different types of high-grade prostatic carcinoma. Histopathology 25: 269-273, 1994.
26. Aihara M, Truong LD, Dunn JK, Wheeler TM, Scardino PT and Thompson TC: Frequency of apoptosis bodies positively correlates with Gleason grade in prostate cancer. Hum Pathol 25: 797-801, 1994.
27. Aihara M, Scardino PT, Truong LD, Wheeler TM, Goad JR, Yang G and Thompson TC: The frequency of apoptosis correlates with the prognosis of Gleason grade 3 adenocarcinoma of the prostate. Cancer 75: 522-529, 1995.
28. Staunton MJ and Gaffney EF: Tumor type is a determinant of susceptibility to apoptosis. Am J Clin Pathol 103: 300-307, 1995.
29. Drachenberg CB, Ioffe OB and Papadimitriou JC: Progressive increase of apoptosis in prostatic intraepithelial neoplasia and carcinoma: Comparison between in situ end-labeling of fragmented DNA and detection by routine hematoxylin-eosin staining. Arch Pathol Lab Med 121: 54-58, 1997.
30. Edge SB and Compton CC: The American Joint Committee on Cancer: The 7th edition of the AJCC cancer staging manual and the future of TNM. Ann Surg Oncol 17: 1471-1474, 2010.
31. Mottet N, Bellmunt J, Bolla M, Briers E, Cumberbatch MG, De Santis M, Fossati N, Gross T, Henry AM, Joniau S, *et al*: EAU-ESTRO-SIOG Guidelines on prostate cancer. Part 1: Screening, diagnosis, and local treatment with curative intent. Eur Urol 71: 618-629, 2017.
32. Reynolds ES: The use of lead citrate at high pH as an electron-opaque stain in electron microscopy. J Cell Biol 17: 208, 1963.
33. Têtu B: Morphological changes induced by androgen blockade in normal prostate and prostatic carcinoma. Best Pract Res Clin Endocrinol Metab 22: 271-283, 2008.
34. Krakhmal NV, Zavyalova MV, Denisov EV, Vtorushin SV and Perelmuter VM: Cancer invasion: Patterns and mechanisms. Acta Naturae 7: 17-28, 2015.
35. Sebastiano C, Vincenzo F, Tommaso C, Giuseppe S, Marco R, Ivana C, Giorgio R, Massimo M and Giuseppe M: Dietary patterns and prostatic diseases. Front Biosci (Elite Ed) 4: 195-204, 2012.
36. Stoff JA: Selected office based anticancer treatment strategies. J Oncol 2019: 7462513, 2019.
37. Hickmen JA: Apoptosis induced by anti-cancer drugs. Cancer Metastasis Rev 11: 121-139, 1992.
38. D'Arcy MS: Cell death: A review of the major forms of apoptosis, necrosis and autophagy. Cell Biol Int 43: 582-592, 2019
39. Li M, Yang X, Wang H, Xu E and Xi Z: Inhibition of androgen induces autophagy in benign prostate epithelial cells. Int J Urol 21: 195-199, 2014.
40. Krajewska M, Krajewski S, Epstein JI, Shabaik A, Sauvageot J, Song K, Kitada S and Reed JC: Immunohistochemical analysis of bcl-2, bax, bcl-X, and mcl-1 expression in prostate cancers. Am J Pathol 148: 1567-1576, 1996.
41. Srivastava SK, Bhardwaj A, Singh S, Arora S, McClellan S, Grizzle WE, Reed E and Singh AP: Myb overexpression overrides androgen depletion-induced cell cycle arrest and apoptosis in prostate cancer cells, and confers aggressive malignant traits: Potential role in castration resistance. Carcinogenesis 33: 1149-1157, 2012.
42. Sun BO, Fang Y, Li Z, Chen Z and Xiang J: Role of cellular cytoskeleton in epithelial-mesenchymal transition process during cancer progression. Biomed Rep 3: 603-610, 2015.
43. Shankar J, Messenberg A, Chan J, Underhill TM, Foster LJ and Nabi IR: Pseudopodial actin dynamics control epithelial-mesenchymal transition in metastatic cancer cells. Cancer Res 70: 3780-3790, 2010.
44. Jolly MK and Celià-Terrassa T: Dynamics of phenotypic heterogeneity associated with emt and stemness during cancer progression. J Clin Med 8: 1542, 2019.